Coherent population dynamics in rubidium atoms excited by resonant 0π pulses

T. Ban, D. Aumiler, S. Vdović, N. Vujičić, H. Skenderović, and G. Pichler
Institute of Physics, Bijenička 46, HR-10 000 Zagreb, Croatia
(Received 12 May 2009; published 28 August 2009)

We investigate the time dynamics of a four-level rubidium atomic system excited by a train of 0π pulses. Resonant 0π pulse shaping is achieved by propagation of weak femtosecond pulses through rubidium vapor and characterized using frequency-resolved optical gating and within the linear dispersion theory. The excitation of the Rb atoms by 0π pulse train is studied experimentally by modified direct frequency comb spectroscopy and theoretically within the density-matrix approach. We show that accumulation of populations and coherences, as typical pulse train excitation effects, strongly depend on the strength of the resonant 0π pulse shaping. Stronger pulse shaping reduces the coherent accumulation effects, eventually leading to the disappearance of the velocity selective optical pumping observed in the frequency domain.

DOI: 10.1103/PhysRevA.80.023425 PACS number(s): 32.80.Qk, 42.50.Gy

I. INTRODUCTION

The goal of coherent control experiments is to control the outcome of a certain physical process through manipulation of interference between different quantum paths [1–3]. Practical implementation of the idea is often complicated by the propagation effects associated with the propagation of pulses through resonant atomic or molecular systems [4,5]. The medium introduces distortions of the input pulse electric field which can be a serious limitation in the coherent control experiments. In order to avoid this undesirable side effect it is crucial to provide information which could help to better understand and, possibly, control the pulse propagation effects.

Zero-area (0π) pulse is obtained as a result of resonant reshaping which occurs when a resonant pulse is propagated through the atomic vapor. 0π pulse is a pulse which leaves the atomic level populations nearly unchanged after its propagation through the medium. The initial part of the pulse excites the atoms and then, as a result of a π phase change in the electric field, the subsequent part of the pulse brings the atoms back to the ground state. This is usually interpreted using two propagation laws. First propagation law states that most of the pulse energy is transmitted when the spectral width of the pulse is larger than the width of the absorption line. The second propagation law is the area theorem, which in the special case of weak fields reduces to the McCall-Hahn theorem [6], stating that the pulse area decreases exponentially with the propagation distance. In order to satisfy these two propagation laws the pulse envelope develops an oscillatory temporal structure. Theoretical [7,8] and experimental [9,10] investigations of the 0π pulses received considerable attention in the literature. However, these investigations have been mostly limited to the reshaping of the nanosecond and picosecond pulses. The first study of resonant, subpicosecond, weak pulses propagating through the sodium vapor was reported in Ref. [11]. The generation of ultrashort pulses in the femtosecond (fs) range opened a new area of investigations of the pulse propagation effects. Due to the wide bandwidth of the fs pulses, the sharp line limit (SLL) and extreme SLL became accessible. With the exception of few experimental studies [12,13], resonant fs pulse propagation effects have been predominantly investigated theoretically [14–16].

The accumulation of populations and coherences occurs as a result of the specific atomic time dynamics when the atomic relaxation times are longer than the time between two consecutive laser pulses. The accumulation effects in two-level Rb atoms excited by a train of fs pulses were theoretically investigated for the first time in Ref. [17]. The extension of this work to three-level rubidium atoms and two-photon excitation was presented in Ref. [18]. The authors discuss the influence of the pulse train parameters and shapes (including 0π pulses) on the accumulation effects in a sequential two-photon transition. Recently, based on coherence accumulation effects, Ye and co-workers at JILA developed direct frequency comb spectroscopy which bridges the fields of high resolution spectroscopy and ultrafast science [19,20].

The accumulation of populations and coherences in room-temperature rubidium vapor excited by fs pulse train was studied extensively in our previous papers [21–23]. The accumulation effects were studied theoretically using the density-matrix approach. The experimental investigations were based on mapping of the frequency comb to the velocity distributions of the hyperfine level populations. We developed modified direct frequency comb spectroscopy (MDFCS) by introducing a weak probe laser in addition to the fs laser. The velocity distributions of the ground state hyperfine level populations are monitored by measuring the probe laser transmission. In our recent paper [24] we introduced the enhanced sensitivity MDFCS and demonstrated it as a powerful technique for characterization of the atomic system excited simultaneously by the cw laser and the fs pulse train. The application of the method for determination of the absolute frequencies of the comb lines was demonstrated recently [25].

The aim of this work is to study the time dynamics of the four-level Rb atomic system excited by the resonantly shaped 0π pulse train. The 0π pulse shaping is achieved as a result of the natural fs pulse reshaping induced by linear dispersion of the absorption line by propagation of resonant weak fs pulses through the rubidium vapor. As the reshaping is strongly dependent on the rubidium atom number density, different pulse shapes are obtained by changing the temperature of the vapor. Characterization of the shaped 0π pulses is

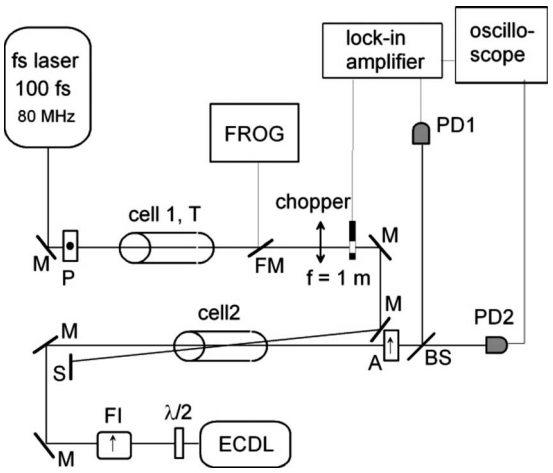

FIG. 1. Experimental scheme: ECDL, external cavity diode laser; FI, Faraday isolator; M, mirror; FM, folded mirror; S, beam stopper; A, analyzer; P, polarizer; PD, photodiode; FROG, experimental setup for SHG-FROG (including BBO crystal); cell 1, pulse reshaping; and cell 2, interaction cell.

performed using frequency-resolved optical gating (FROG) and within the linear dispersion theory. Study of the excitation of rubidium atoms by a train of resonantly shaped 0π pulses is performed in the second cell containing rubidium atoms at room temperature. We emphasize the effect of the 0π pulse train excitation on the time evolution of the atomic ground and excited state populations. We show that accumulation of populations and coherences strongly depends on the strength of the resonant shaping. By increasing the strength of the pulse shaping, the accumulation effects reduce, leading to the disappearance of the velocity selective optical pumping (VSOP) observed in the frequency domain. In addition, we demonstrate the advantage of the MDFCS technique over FROG technique in sensing the small modification of the pulse caused by resonant shaping of the fs pulse induced by its propagation through the low-density rubidium vapor.

II. EXPERIMENT

The experimental setup (Fig. 1) is based on the MDFCS setup [24] with an additional Rb cell placed on the path of the fs laser beam. Briefly, a mode-locked Ti:sapphire laser (Tsunami, Spectra Physics) with pulse duration of about 100 fs and pulse repetition of 80 MHz adjusted at the 795 nm peak wavelength is used for the rubidium atom excitation. The fs laser beam is sent through the first Rb cell (cell 1) and then weakly focused into the center of the second cell (cell 2). We used the cell containing natural abundance of the rubidium isotopes (72% ^{85}Rb and 28% ^{87}Rb) or the cell containing pure ^{87}Rb isotope as the first cell. All cells are 5 cm long with the outer diameter of 2.5 cm. Cell 1 is placed in an oven enabling us to control the temperature, i.e., rubidium number density in the cell. Cell 2 is kept at room temperature ($T=293$ K, $N_{\mathrm{Rb}}=5.4\times10^{9}$ cm^{-3}). In addition to the fs laser beam, a weak cw probe laser (Toptica DL100, ECDL at 780 nm) propagating anticollinearly with the fs laser is sent through cell 2. The probe and fs laser beams are intersected in the center of cell 2 under a small angle. The probe laser frequency is slowly scanned across the Doppler-broadened ^{85,87}Rb $5\,^2S_{1/2}\rightarrow5\,^2P_{3/2}$ hyperfine transitions at 3 GHz/s scanning rate. Its transmission is simultaneously measured with two Hamamatsu Si photodiodes. The signal from the first photodiode is fed in the lock-in amplifier (Stanford Research SR510) referenced to the SR540 mechanical chopper at 3.5 kHz (positioned on the fs laser beam). Measured signal represents the change in the probe laser transmission, ΔT, induced by the fs laser excitation. Here, $\Delta T=T_{\mathrm{fs}}-T$, where T_{fs} and T are the probe laser transmission with and without the fs pulse train excitation, respectively. The signal from the lock-in amplifier was stored into a digital oscilloscope (Tektronix TDS5140). The signal from the second photodiode PD2 was directly fed into a digital oscilloscope and it measured the probe laser transmission across all four Doppler-broadened $5\,^2S_{1/2}\rightarrow5\,^2P_{3/2}$ absorption lines at 780 nm.

The FROG measurements were performed using the second-harmonic signal from a nonlinear 100-μm-thick beta barium borate (BBO) crystal. The second-harmonic generation (SHG) signal of the beam after the first cell was autocorrelated and spectrally resolved in the compact charge-coupled device spectrometer (Ocean Optics, HR2000) with a 200–420 nm wavelength range and a spectral resolution of about 0.2 nm. One of the pulse replicas was delayed using a delay stage. The temporal resolution given by the delay stage minimal step size was 2 fs.

III. RESULTS AND DISCUSSION

We investigated experimentally the accumulation of coherences and populations in rubidium atoms excited by the resonant 0π pulse train. 0π pulses were generated in cell 1 by propagation of weak near Fourier-limited fs pulses through resonant rubidium vapor. The generation of the 0π pulses is discussed in Sec. III A. The interaction of resonant 0π pulse train and rubidium atoms at room temperature (cell 2) is investigated in Sec. III B.

A. Generation of resonant 0π pulses

1. Propagation of an fs pulse through the resonant rubidium vapor

In the case of low-energy pulses, the pulse reshaping by resonant interaction is practically independent of the pulse energy and the classical linear dispersion theory can be applied [12,26]. The propagation of the pulse in the $+z$ direction through a dispersive medium is described by the following relation [27]:

$$\tilde{E}(\omega,z)=\tilde{E}(\omega,0)e^{-ik(\omega)z}. \tag{1}$$

Here $\tilde{E}(\omega,z)$ is the complex spectrum of the pulse. $\tilde{E}(\omega,0)$ is calculated as a complex Fourier transform of the pulse electric field, taken as a real hyperbolic-secant function. $k(\omega)$ is the wave vector given by $k(\omega)=\frac{\omega}{c}n(\omega)$, where ω is the frequency and $n(\omega)$ is the frequency dependent complex refractive index of the material. In the case of low-energy resonant

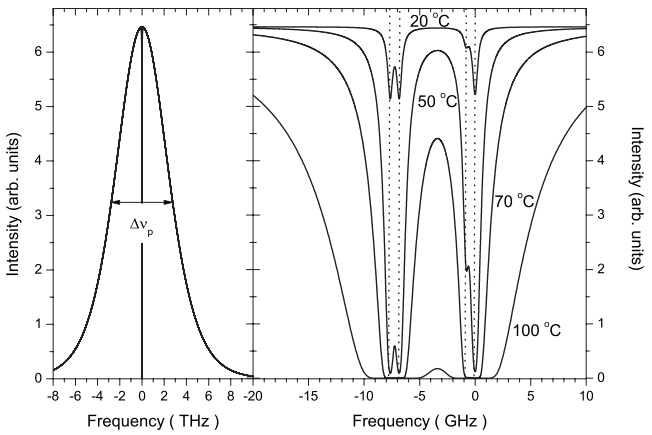

FIG. 2. Left panel: calculated pulse spectra of the weak fs pulse propagated through the resonantly $[5\,^2S_{1/2}(F_g=1)\rightarrow 5\,^2P_{1/2}(F_e=2)]$ excited 5-cm-long column of ^{87}Rb low-density atomic vapor. The initial pulse shape is assumed to be hyperbolic-secant pulse with the electric field amplitude of 1×10^6 V/m and FWHM of 2817 GHz corresponds to the 100 fs Fourier-limited pulses. Right panel: calculated pulse spectra of the weak fs pulse for the narrow frequency range around pulse center.

pulses propagating through low-density rubidium vapor, $n(\omega)$ can be calculated using a classical dispersion formula [28],

$$n(\omega) = 1 + \frac{Ne^2}{2\varepsilon_0 m_e}\sum_{j=1}^{4} f_j \frac{1}{\omega_j^2 - \omega^2 + i\gamma_j\omega}. \qquad (2)$$

Here, N is the concentration of Rb atoms, e is the electron charge, m_e is the electron mass, and ω_j are frequencies of the electronically allowed ^{87}Rb $5\,^2S_{1/2}(F_g=1,2)\rightarrow 5\,^2P_{1/2}(F_e=1,2)$ transitions [29] with the corresponding linewidths γ_j and oscillator strengths f_j [30]. Since the experiments were performed in the conditions of low-density rubidium vapor (SLL), we are considering only homogeneous broadening and as a crude approximation take the absorption linewidth γ as the sum of three terms $\gamma=\gamma_n+\gamma_{coll}+\gamma_{Doppler}$ [13]. γ_n is the natural linewidth equal to 5.746 MHz [31], γ_{coll} is the collision-induced line broadening, and $\gamma_{Doppler}$ is the Doppler width equal to 500 MHz for the room-temperature atoms [32]. Since in the experimental conditions of low-density Rb vapor (N_{Rb} below 5×10^{12} cm^{-3}) and evacuated Rb cell the absorption linewidth γ is dominated by the Doppler width (γ_{coll} can be deduced from the experimental values for self-broadening of the Rb $5\,^2S_{1/2}\rightarrow 5\,^2P_{1/2}$ resonance line [32] and at highest experimental temperature of 100 °C is equal to 18 MHz) it is reasonable to take $\gamma_j=\gamma_{Doppler}$ $(j=1,2,3,4)$ in the case of all four Rb $5\,^2S_{1/2}(F_g=1,2)\rightarrow 5\,^2P_{1/2}(F_e=1,2)$ transition lines.

In Fig. 2 we show calculated spectrum of a resonant weak fs pulse after propagation of 5 cm through low-density rubidium vapor at different temperatures. The initial hyperbolic-secant pulse with electric field amplitude of 1×10^6 V/m was used. Taking into account the $5\,^2S_{1/2}\rightarrow 5\,^2P_{1/2}$ transition dipole moment (2.537×10^{-29} C m [31]), calculated pulse area corresponds to 0.014π (weak pulse regime). The pulse spectrum is centered at ^{87}Rb $5\,^2S_{1/2}(F_g=1)\rightarrow 5\,^2P_{1/2}(F_e=2)$ transition frequency, with the full width at half maximum (FWHM) equals 2817 GHz (corresponding to a 100 fs Fourier-limited *sech* pulse). The absorption is observed only in the narrow frequency range around the center of the pulse, so only the central part of the spectra is shown in the right panel of Fig. 2. Vapor temperatures were deduced from the rubidium atom densities using the Nesmeyanov vapor pressure curves [33]. The observed absorption pattern consists of four ^{87}Rb resonance lines (two lines coming from the $F_g=1$ ground state hyperfine level and the other two coming from the $F_g=2$ level) broadened by the Doppler effect. Even at room temperature, four lines are not completely resolved. By increasing the temperature the lines become broader and, finally, they merge into a wide and optically thick absorption line.

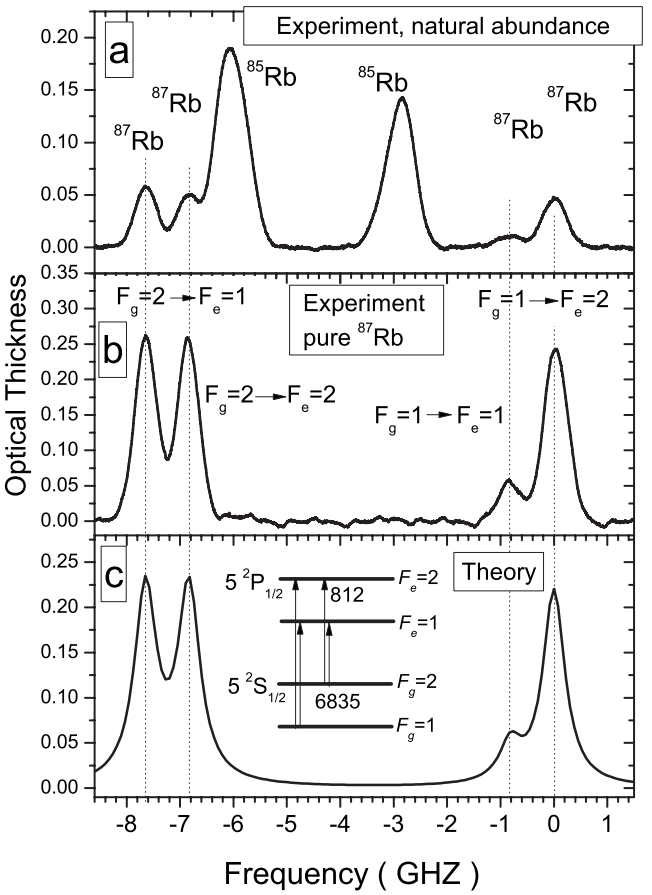

FIG. 3. Comparison of the experimental and theoretical absorption spectra of room-temperature rubidium vapor: (a) experimental optical thickness of the rubidium isotopic mixture in the natural abundance; (b) experimental optical thickness of the pure ^{87}Rb isotope; and (c) calculated optical thickness of the pure ^{87}Rb isotope.

In order to test the propagation results, we compare calculated and measured rubidium vapor optical thickness. The results for the rubidium vapor at room temperature are shown in Fig. 3. In the experiment, the transmission of a weak cw laser diode (Toptica, LD-0795-0150-2, nominal wavelength of 795 nm) scanned across the Doppler-broadened absorption profiles was measured. Measurements were performed for the cell containing natural abundance of

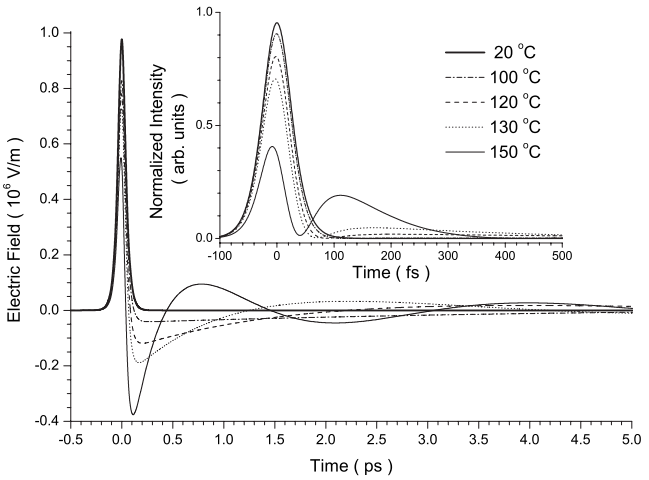

FIG. 4. Real part of the 0π pulse electric field retrieved from the pulse spectrum presented in Fig. 2 by applying the inverse Fourier transform. Inset: corresponding 0π pulse intensity profiles.

the rubidium isotopes [Fig. 3(a)] and the cell containing pure ^{87}Rb isotope [Fig. 3(b)]. Theoretical optical thickness [Fig. 3(c)] is given by the imaginary part of the complex refraction index [32] [see Eq. (2)]. It can be observed that the theoretical spectrum well reproduces measured Rb D_1 line at 795 nm.

Electric field of the resonantly shaped pulses (Fig. 4) is calculated as the inverse Fourier transform of the pulse spectra shown in Fig. 2. The reshaping of the pulse during its propagation through the vapor has been observed by increasing the temperature of the vapor (rubidium atom density). It is manifested as the large extension of the pulse wing followed by the oscillatory structure of the electric field envelope at higher Rb atom number densities (ringing in the pulse tail). Our calculations show that even at low rubidium atom number densities (for example, 100 °C on Fig. 4) the considerable pulse broadening up to 20 ps appears. The inset of Fig. 4 displays the corresponding intensities. The total energy of the pulse remains essentially constant as the temperature is increased, while the peak intensity decreases due to the pulse broadening. The shapes of the obtained intensity profiles with an additional oscillation are similar to the one obtained in Ref. [11] observed for similar optical densities. However, in Ref. [11] the propagation of the 0.5 ps pulses through sodium vapor was considered and consequently the observed pulse reshaping occurs at picosecond time scale.

2. Pulse characterization using the FROG technique

The characterization of the resonantly shaped fs pulses was investigated experimentally by the FROG technique. The fs laser spectrum was centered at 795 nm (corresponding to $5\ ^2S_{1/2} \rightarrow 5\ ^2P_{1/2}$ excitation) with average input power of 400 mW (5 nJ/pulse). We observed that FROG traces measured at temperatures below 100 °C ($N_{\mathrm{Rb}}=5\times10^{12}$ cm^{-3}) do not show any difference from the FROG trace measured at room temperature. This implies that at low rubidium densities the shaping is very weak and the effect of such weak shaping could not be observed in FROG traces. FROG traces

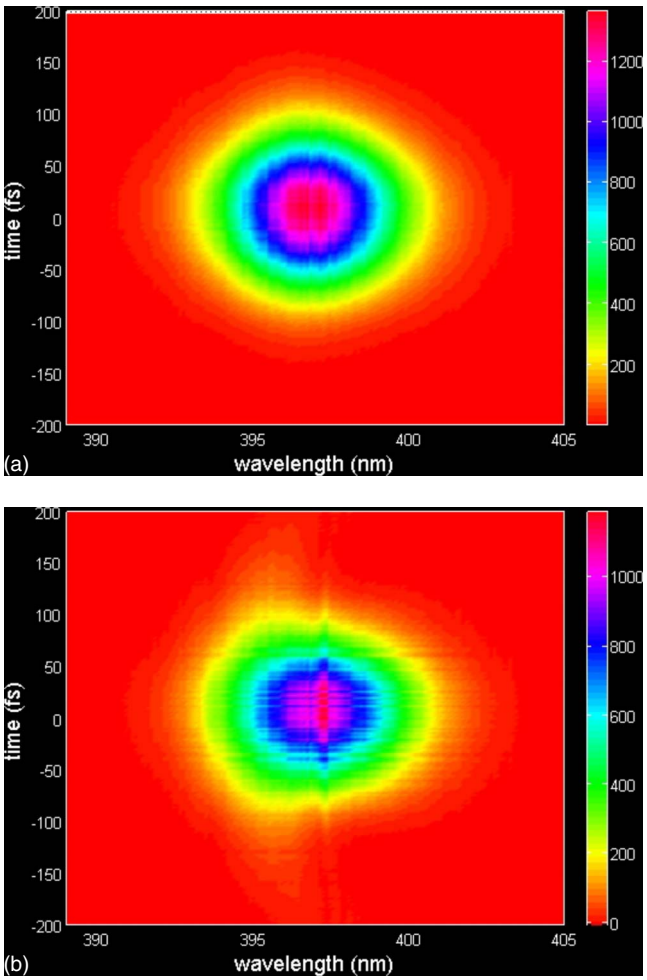

FIG. 5. (Color online) SHG-FROG traces at (a) 24 °C and (b) 115 °C after propagation of the weak 100 fs pulse through the 5-cm-long column of rubidium vapor. The fs laser is centered at 795 nm (corresponding to $5\ ^2S_{1/2} \rightarrow 5\ ^2P_{1/2}$ excitation).

obtained for the fs pulses propagating through rubidium vapor at 24 and 115 °C are shown in Figs. 5(a) and 5(b), respectively. The FROG trace measured at 24 °C shows a typical pattern usually obtained for the Fourier-limited hyperbolic-secant pulses [27]. The FROG trace measured at 115 °C differs from one measured at 24 °C, reflecting the change in the electric field during pulse propagation. Its horizontal cuts, which represent the FROG-SHG spectra at different delay times, exhibit a narrow spike positioned exactly in the center of the spectra. Similar FROG trace was observed in Ref. [34], where the propagation of 100 fs pulses centered at 780 nm through Rb vapor was investigated. The authors compare experimental and calculated SHG-FROG spectra, but no pulse characterization using FROG-retrieval program was performed. In our case, the pulse reconstruction from measured FROG trace at 115 °C by using a FROG-retrieval computer program did not show quantitative agreement with the theoretical results. This is reasonable since we investigated the reshaping effect induced by linear dispersion of the absorption line in the condition of low-density vapor characterized by very small width of the absorption line (for example, at $T=100$ °C, $\Delta\lambda$ is about 0.04 nm; see Fig. 2). In

order to measure the spectral structure of 0.04 nm in the pulse with the FROG technique, one should have ~0.02 nm of spectral resolution or better. This would be difficult to achieve even with the high resolution spectrometers. The FROG technique is therefore not practically applicable for the characterization of the pulses shaped by the propagation through low-density atomic media.

B. Coherent accumulation effects

1. Time domain

The influence of the resonant 0π pulse train excitation on the coherent accumulation of populations and coherences was calculated utilizing the theoretical approach described in detail in our previous papers [21,22,24]. The model is based on the standard density-matrix analysis, starting from the Liouville equation, with appropriate modifications which include the repopulation of the ground states due to the spontaneous decay of the excited states.

The four-level (two $5\ ^2S_{1/2}$ hyperfine ground levels and two $5\ ^2P_{1/2}$ excited hyperfine levels) ^{87}Rb atoms interacting with the 0π pulse train electric field are considered. The density-matrix equations of motion are given by [35]

$$\dot{\rho}_{nm} = -i\hbar^{-1}[\hat{H},\hat{\rho}]_{nm} - \gamma_{nm}\rho_{nm}, \quad n \neq m,$$

$$\dot{\rho}_{nn} = -i\hbar^{-1}[\hat{H},\hat{\rho}]_{nn} + \sum_{m(E_m>E_n)} \Gamma_{nm}\rho_{mm} - \sum_{m(E_m<E_n)} \Gamma_{mn}\rho_{nn}, \tag{3}$$

where the subscripts nm refer to the four hyperfine levels numbered from the lowest to highest-energy level. Γ_{nm} gives the population decay rate from level m to level n and γ_{nm} is the damping rate of the ρ_{nm} coherence. In low-density rubidium vapor at room temperature, the radiative decay rates dominate all damping rates [21,22].

The Hamiltonian of the system is $\hat{H}=\hat{H}_0+\hat{H}_{\text{int}}$, where $\hat{H}_0$ is the Hamiltonian of the free atom and $(H_{\text{int}})_{nm} = -\mu_{nm}E_{0\pi}(t)$ represents the interaction of the atom with the electric field of the 0π pulse train. μ_{nm} is the dipole moment of the electronically allowed $(F_g \rightarrow F_e=F_g,\ F_g \pm 1)$ transitions, calculated from Ref. [30]. 0π pulse train electric field, $E_{0\pi}(t)$, is taken as a sequence of pulses obtained as a result of the weak resonant fs pulse propagation through low-density rubidium vapor (as described in paragraph 3.1.1.). From Eq. (3) a system of ten coupled differential equations for the slowly varying density-matrix elements is obtained. The population of the nth atomic level is given by the diagonal density-matrix element ρ_{nn}, whereas off diagonal elements ρ_{nm} represent coherences. The resulting system of coupled differential equations was integrated using a standard fourth-order Runge-Kutta method.

Time evolutions of ground, $5\ ^2S_{1/2}$, and excited, $5\ ^2P_{1/2}$, ^{87}Rb hyperfine level populations induced by the resonant 0π pulse train excitation are shown in Figs. 6 and 7, respectively. The calculations were performed for the 0π pulse electric fields, obtained by dispersion theory approach (see paragraph 3.1.1.) considering the propagation of the weak hyperbolic-secant pulse with electric field amplitude of 1×10^6 V/m and pulse duration of 100 fs through the rubidium vapor at 20 and 50 °C (cell 1). The pulse central frequency was set in resonance with ^{87}Rb $5\ ^2S_{1/2}(F_g=1) \rightarrow 5\ ^2P_{1/2}(F_e=2)$ hyperfine transition. In Fig. 7 only the population of resonantly excited $5\ ^2P_{1/2}(F_e=2)$ hyperfine level is shown. The excitation of the ^{87}Rb atoms by resonant 0π pulse train generated after the propagation of the fs pulses through rubidium vapor at 20 °C yields the population time evolutions similar to those obtained for Fourier-

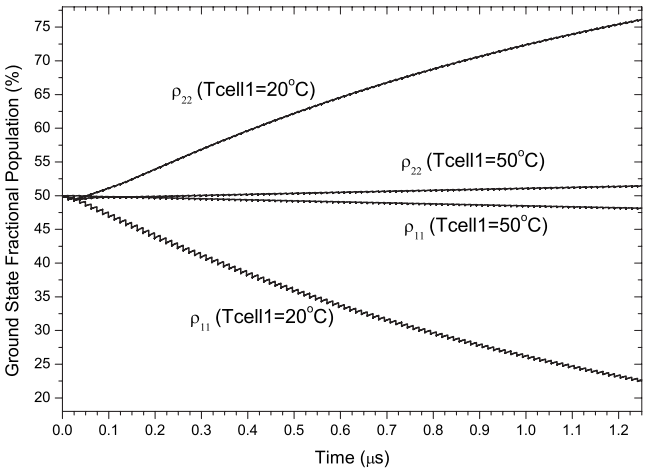

FIG. 6. Calculated time evolutions of the ^{87}Rb ρ_{11}, ρ_{22} ground state hyperfine level populations in the case of resonant interaction with the 0π pulse train. 0π pulses are generated after the propagation of weak 100 fs Fourier-limited sech pulses through the 5-cm-long column of ^{87}Rb atoms vapor at two different temperatures of cell 1 (cell 1 at 20 °C and cell 1 at 50 °C). The central pulse frequency was set in resonance with ^{87}Rb $5\ ^2S_{1/2}(F_g=1) \rightarrow 5\ ^2P_{1/2}(F_e=2)$ hyperfine transition.

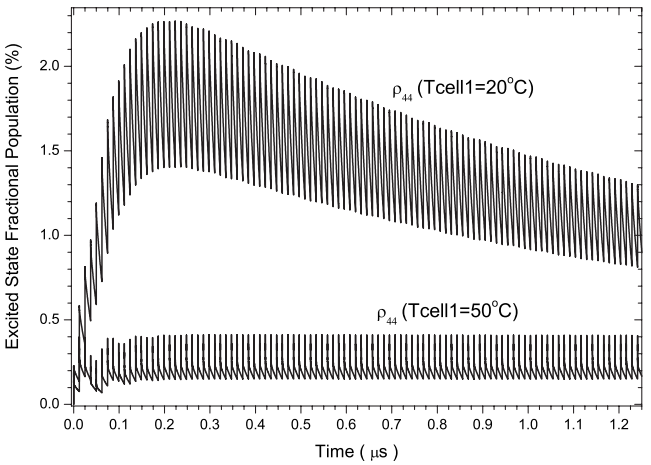

FIG. 7. Calculated time evolution of the ^{87}Rb ρ_{44} excited state hyperfine level populations in the case of resonant interaction with the 0π pulse train. 0π pulses are generated after the propagation of weak 100 fs Fourier-limited sech pulses through the 5-cm-long column of ^{87}Rb atoms vapor at two different temperatures of cell 1 (cell 1 at 20 °C and cell 1 at 50 °C). The central pulse frequency was set in resonance with ^{87}Rb $5\ ^2S_{1/2}(F_g=1) \rightarrow 5\ ^2P_{1/2}(F_e=2)$ hyperfine transition.

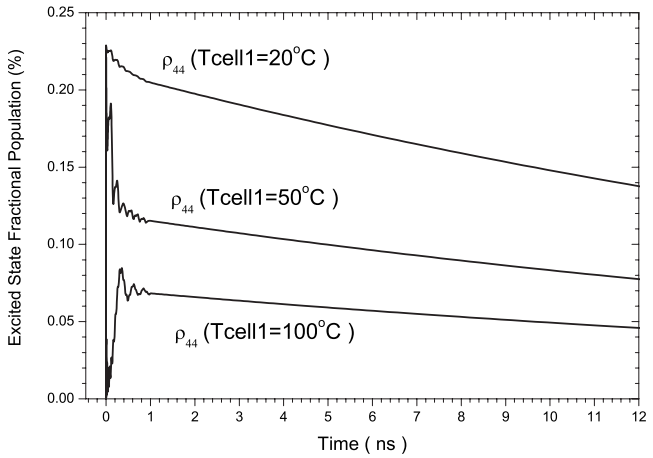

FIG. 8. Calculated ^{87}Rb ρ_{44} single 0π pulse excitation population dynamics. 0π pulses are generated after the propagation of weak 100 fs Fourier-limited sech pulses through the 5-cm-long column of ^{87}Rb atoms vapor at different temperatures of cell 1 (cell 1 at 20 °C, cell 1 at 50 °C, and cell 1 at 100 °C). The central pulse frequency was set in resonance with ^{87}Rb $5\,^2S_{1/2}(F_g=1) \rightarrow 5\,^2P_{1/2}(F_e=2)$ hyperfine transition.

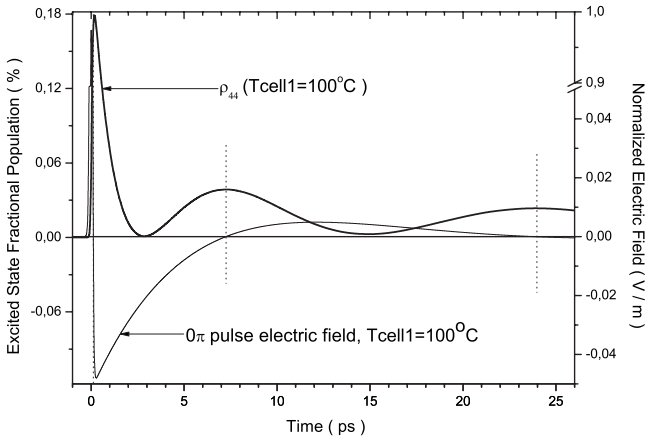

FIG. 9. Calculated ^{87}Rb excited level population ρ_{44} together with the corresponding 0π pulse electric field (real part) used for excitation. 0π pulses are generated after propagation through cell 1 at 100 °C. The central pulse frequency was set in resonance with ^{87}Rb $5\,^2S_{1/2}(F_g=1) \rightarrow 5\,^2P_{1/2}(F_e=2)$ hyperfine transition.

limited pulses [21,22,24]. This is understandable since at 20 °C the rubidium atom number density is too low to induce considerable pulse reshaping and the electric field after propagation remains almost identical to the electric field of the input hyperbolic-secant pulse (see Fig. 4). The atoms can never completely relax between two consecutive pulses and accumulate excitation in the form of excited state populations and coherences. Although the stationary state is achieved on a time scale of about 10 μs, we only show the time evolution up to 1.25 μs, which is the average interaction time of the atoms within the fs laser beam.

By increasing the rubidium number density in cell 1, the strength of resonant reshaping increases, i.e., the shape of the pulses changes. It is therefore expected that the excitation of the Rb atoms in cell 2 by such, more reshaped, 0π pulse train yields to different time evolution of the atomic system. This is clearly demonstrated in Figs. 6 and 7, where calculated population time evolutions for the 0π pulse train resonantly shaped at 50 °C (cell 1) are presented. Although the population excited by a single pulse is still evident, accumulation of population in the excited level is strongly suppressed at 50 °C (see Fig. 7), indicating that even the weak resonant pulse shaping strongly reduces the coherent accumulation effects. The reduction in the accumulation of population in the excited state is responsible for a less efficient optical pumping process (reduction in the ground state hyperfine population difference; see Fig. 6). Time evolutions of the excited state hyperfine level populations, ρ_{44}, calculated for the excitation of ^{87}Rb atoms by differently shaped 0π pulse trains in the time between two consecutive pulses (namely, the time between the first and the second pulses) are shown in Fig. 8. Different 0π pulse shapes are obtained by the propagation of the fs pulse through Rb vapor at different temperatures. The remarkable sensitivity of the excited state hyperfine level populations, ρ_{44}, on the 0π pulse shape is evident. Although the 0π pulse shape has not be changed significantly for the pulse propagated through cell 1 at 20 and 100 °C (see Fig. 4), the ρ_{44} final population (population before the consequent pulse) decreased three times. At the beginning, the excited level populations follow the 0π pulse electric field. Later, after the passage of the 0π pulse the time dynamics is governed by the spontaneous decay. For higher temperatures of cell 1 (larger atom number densities), generated 0π pulses exhibit extension of the pulse wing with appropriate ringing, accompanied by the electric field amplitude decrease (see Sec. III A 1). This behavior is directly imprinted into the excited level population dynamics and explains the reduced population excited by the single pulse.

In order to illustrate this behavior in more detail, the ^{87}Rb excited level population together with the corresponding 0π pulse electric field envelope [real part of $\tilde{E}(t)$] used for excitation is shown in Fig. 9. This figure verifies the real physical nature of the 0π pulse. The initial part of the 0π pulse excites the atoms resulting in the ρ_{44} increase. Then, as a result of π phase change in the electric field, the later part of the pulse takes the atoms back to the ground state (decrease in ρ_{44}). As the electric field further oscillates in sign, the atomic excited level population oscillates in time between some maximum value and zero with the final population determined by the strength of the 0π pulse shaping. In the case of the considerably shaped 0π pulse the final excited level population that is equal to zero is observed, leaving the atoms in the same (ground) state as they were before the interaction.

2. Frequency domain

In order to compare experiments and theory we have to transform the theoretical results obtained in the time domain to the analogous results in the frequency domain. In Doppler-broadened vapor, the atomic transition frequency ω_{ge} has to be replaced with $\omega'_{ge}=\omega_{ge}+\vec{k}\cdot\vec{v}$, where $\vec{k}$ is the laser wave vector and $\vec{v}$ is the atomic velocity. We solved density-matrix equations of motion for each velocity group and calculated

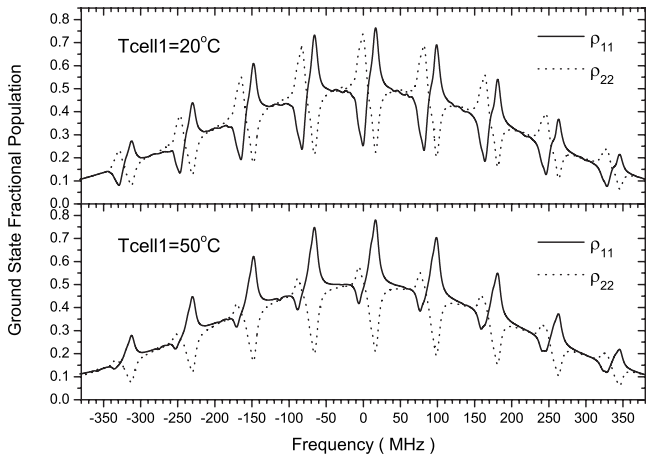

FIG. 10. Calculated Doppler-broadened ^{87}Rb ground state hyperfine level populations, ρ_{11} and ρ_{22}, for different atomic velocity groups in the case of resonant ($5\,^2S_{1/2} \rightarrow 5\,^2P_{1/2}$) 0π pulse train excitation. Shown results are obtained for the 0π pulses generated after propagation through cell 1 at 20 °C (upper panel) and 50 °C (lower panel).

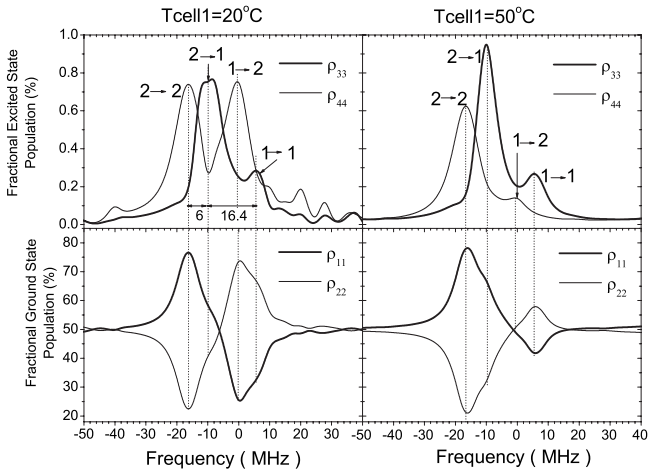

FIG. 11. Calculated ground (ρ_{11}, ρ_{22}) and excited (ρ_{33}, ρ_{44}) state hyperfine level populations in one period of modulations, induced by 0π pulse train resonant excitation. The results are calculated for 0π pulses generated after propagation through cell 1 at 20 °C (left panels) and 50 °C (right panels).

ground and excited level populations together with coherences. Final populations are taken to be the population at 1.25 μs, which is the average interaction time of the atoms with the fs laser beam cross section [22]. The atomic velocity distributions of the ^{87}Rb ($F_g=1,2$) ground state hyperfine level populations, ρ_{11} and ρ_{22}, calculated for the 0π pulse excitation are shown in Fig. 10. The upper panel corresponds to the 0π pulses generated after propagation through cell 1 at 20 °C (negligible shaping), whereas the lower panel corresponds to the 0π pulse generated after propagation through cell 1 at 50 °C (significant shaping). In the case of negligible shaping, the VSOP influenced by the accumulation of population in the time domain (due to the pulse train excitation) is clearly evident. This phenomenon has been extensively investigated in our previous papers [21,22,24]. The characteristic periodic oscillations of the hyperfine level population distributions with two-peak structure (one minimum and one maximum) in one period are obtained. This behavior is expected since the 0π pulse shaping with cell 1 at 20 °C is very weak and the shaped pulse is almost identical to the input pulse (see Fig. 4). The shape of the population distribution is determined by the ^{87}Rb ground ($5\,^2S_{1/2}$) and excited ($5\,^2P_{1/2}$) state hyperfine energy level splittings and appropriate transition dipole moments. The periodicity of the population distributions is determined by the pulse repetition rate. On the other hand, the significant shaping of the pulses after their propagation through cell 1 at 50 °C changes the shape of the ground state hyperfine level population distributions. The excitation of atoms in the velocity group possessing a minimum in ρ_{11} (or a maximum in ρ_{22}) is strongly suppressed resulting in the smaller population transfer due to the optical pumping. Therefore, the minima in ρ_{11} (and maxima in ρ_{22}) are less pronounced. In order to explain this behavior in more detail we present in Fig. 11 one period distribution (~80 MHz range) of calculated hyperfine level populations. The hyperfine splitting of the ground $5\,^2S_{1/2}$ state, 6834.6 MHz, is 16.4 MHz detuned from the multiple of 80.6 MHz, repetition rate, whereas the hyperfine splitting of the excited $5\,^2P_{1/2}$ state (812 MHz) is only 6 MHz detuned from the multiple of 80.6 MHz. Therefore, $5\,^2S_{1/2}(F_g=1) \rightarrow 5\,^2P_{1/2}(F_e=1,2)$ excitations occur for velocity groups of atoms detuned by 6 MHz, while $5\,^2S_{1/2}(F_g=1) \rightarrow 5\,^2P_{1/2}(F_e=1)$ and $5\,^2S_{1/2}(F_g=2) \rightarrow 5\,^2P_{1/2}(F_e=1)$ excitations occur for the velocity groups of atoms detuned by 16.4 MHz. As a result, the comblike populations in the excited state hyperfine levels are observed and clearly demonstrated in Fig. 11. These comblike populations in the excited state levels determine, through the optical pumping process, the populations of the ground state levels. Minimum (maximum) and maximum (minimum) in the ρ_{11} (ρ_{22}) come predominately as a result of the $5\,^2S_{1/2}(F_g=1) \rightarrow 5\,^2P_{1/2}(F_e=2)$ and $5\,^2S_{1/2}(F_g=2) \rightarrow 5\,^2P_{1/2}(F_e=2)$ transitions. In the case of the significant pulse shaping (cell 1 at 50 °C), the $5\,^2S_{1/2}(F_g=1) \rightarrow 5\,^2P_{1/2}(F_e=2)$ excitation is strongly suppressed and the minimum (maximum) in ρ_{11} (ρ_{22}) is determined only by the $5\,^2S_{1/2}(F_g=1) \rightarrow 5\,^2P_{1/2}(F_e=1)$ transition (with smaller transition dipole moment). This suppression comes as a result of the 0π pulses excitation (see Fig. 8). In addition, an interesting shape of the $5\,^2S_{1/2}(F_g=2) \rightarrow 5\,^2P_{1/2}(F_e=1)$ excitation line (ρ_{33}) with the small dip in the line center is observed in the case of negligible shaping (cell 1 at $T=20$ °C), whereas for significantly shaped pulses (cell 1 at $T=50$ °C) the dip disappears and larger population (25% increase) is observed at line center (higher excitation efficiency). Our preliminary results lead to the conclusion that the dip in $5\,^2S_{1/2}(F_g=2) \rightarrow 5\,^2P_{1/2}(F_e=1)$ line comes as a result of the electromagnetically induced transparency process. However, this interesting phenomenon has to be further investigated and the detailed discussion will be the scope of some future paper.

The experimental results concerning the interaction of the Rb atoms with the resonantly shaped pulse train are shown in Fig. 12. The fs pulses propagated through cell 1 containing pure ^{87}Rb vapor at different temperatures and 0π pulses are

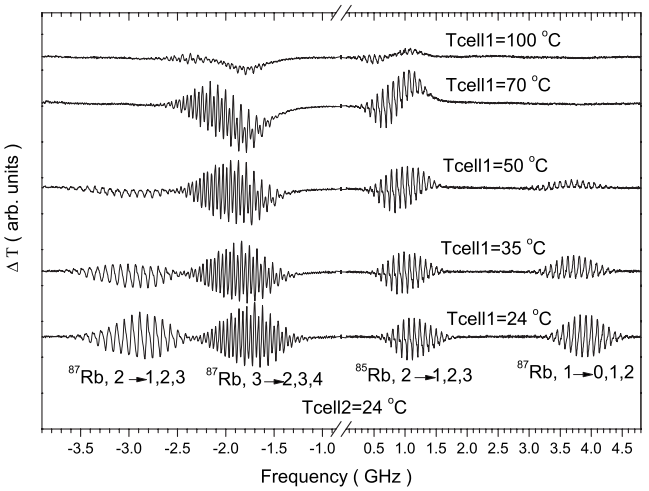

FIG. 12. Dependence of the changes in the probe laser transmission, ΔT, induced by 0π pulse train excitation upon the strength of the 0π pulse shaping (i.e., temperature of cell 1 containing pure ^{87}Rb isotope). The shaped 0π pulses interact with rubidium atoms in cell 2 containing rubidium isotopic mixture in the natural abundance. The probe laser was scanned across $5\ ^2S_{1/2} \rightarrow 5\ ^2P_{3/2}$ rubidium absorption line at 780 nm.

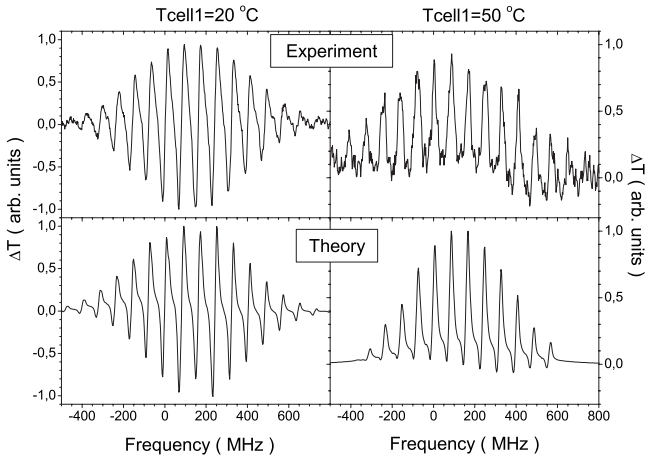

FIG. 13. Comparison between measured and calculated ΔT for ^{87}Rb $5\ ^2S_{1/2}(F_g=1) \rightarrow 5\ ^2P_{1/2}(F_e=0,1,2)$ transition line.

generated. The excitation of the Rb atoms by 0π pulse train is performed in cell 2 containing both rubidium isotopes (natural abundance) using MDFC technique. The probe laser is scanned across all four $5\ ^2S_{1/2} \rightarrow 5\ ^2P_{3/2}$ Doppler-broadened absorption lines and the changes in the probe laser transmission (ΔT) induced by the fs laser excitation are measured. Typical modulation structure, already described and interpreted in our previous paper [24], is observed in the case of negligible shaping (cell 1 at 24 °C). By increasing the temperature of cell 1, the modulation structure (ΔT) of the ^{87}Rb isotope changes. The modulations of the ^{87}Rb $5\ ^2S_{1/2}(F_g=1) \rightarrow 5\ ^2P_{3/2}(F_e=0,1,2)$ absorption profile become predominantly positive, while the modulations of the $5\ ^2S_{1/2}(F_g=2) \rightarrow 5\ ^2P_{3/2}(F_e=1,2,3)$ absorption profile become negative. By further increasing the temperature of cell 1, i.e., stronger resonant pulse shaping, the fs laser ceases to affect the probe laser transmission observed on ^{87}Rb absorption lines (no modulations are observed) and simultaneously, the dispersive-type shape of the modulation structure on ^{87}Rb absorption lines is observed.

In order to compare experiments and theory we calculated ΔT as a difference of the probe laser transmission with, T_{fs}, and without the fs laser, T. The transmission of the probe laser is calculated using Beer-Lambert low [32]. Due to the linear absorption regime, the optical thickness can be deduced from the calculated ground state hyperfine levels populations (ρ_{11} and ρ_{22}, shown in Fig. 10). One absorption profile consists of three hyperfine transition lines; therefore to calculate one absorption profile we have to add all three components with the appropriate frequency detunings and relative transition dipole moments. The comparison between experimental and simulated ΔT for the ^{87}Rb $5\ ^2S_{1/2}(F_g=1) \rightarrow 5\ ^2P_{3/2}(F_e=0,1,2)$ absorption profile in the case of the 0π pulse train excitation is shown in Fig. 13. The left panel corresponds to the 0π pulse generated after the propagation through the first cell containing ^{87}Rb isotope at 24 °C, whereas the right panel corresponds to the first cell at 50 °C. The agreement between theory and experiment is satisfactory.

As we have shown, the excitation of the atoms by significantly shaped 0π pulses changes the excited state population time dynamics (see Fig. 7). Although the relaxation times of the system remain the same, 0π pulse train excitation does not lead to the accumulation of populations (and consequently coherences). In the experiment this is demonstrated as an absence of the modulations in ΔT for higher temperatures of the first cell.

IV. CONCLUSION

Resonant 0π pulse shaping induced by the propagation of weak fs pulses through low-density rubidium vapor is investigated theoretically using linear dispersion theory and experimentally using FROG. 0π pulses are generated as a result of the natural fs pulse reshaping induced by linear dispersion of absorption line. This reshaping is strongly dependent on the rubidium atom density. Therefore, by changing the temperature of the vapor, 0π pulses with characteristic large extension of the pulse wing followed by the oscillatory structure of the electric field envelope are obtained. Our calculations show that even for low rubidium atom number density the considerable extension of the pulse electric field envelope up to 20 ps appears.

We investigated the influence of the resonant 0π pulse shaping on the coherent accumulation effects. We calculated the time dynamics of the rubidium system excited by the resonantly shaped 0π pulse train and demonstrated the suppression of accumulation effects as the strength of the shaping is increased. In the experiment, this is manifested through disappearance of the modulations in the probe laser transmission. The simulations of the experimental spectra are performed, demonstrating satisfactory agreement and confirming the validity of the presented theoretical model. We have shown that the propagation effects in a resonant medium cannot be neglected even in the conditions of low-density vapor.

In addition, we have demonstrated the remarkable sensitivity of the MDFCS technique on the strength of the resonant 0π pulse shaping. In particular, we stress the advantage of the MDFCS technique over the FROG technique in sensing the small changes in the pulse shapes which are induced by resonant shaping in low-density atomic vapors. We believe that this exceptional sensitivity of the MDFC spectroscopy could be used to monitor the pulse shaping in various systems where the shaping due to pulse propagation is weak but still undesirable.

ACKNOWLEDGMENTS

We acknowledge the support from the Ministry of Science, Education and Sports of the Republic of Croatia (Project No. 035-0352851-2857) and Alexander von Humboldt Foundation.

[1] P. Brumer and M. Shapiro, Chem. Phys. Lett. **126**, 541 (1986).
[2] R. Netz, T. Feurer, G. Roberts, and R. Sauerbrey, Phys. Rev. A **65**, 043406 (2002).
[3] D. Felinto, L. H. Acioli, and S. S. Vianna, Opt. Lett. **25**, 917 (2000).
[4] C. Chen and D. S. Elliot, Phys. Rev. A **53**, 272 (1996).
[5] M. A. Bouchene, J. C. Delagnes, M. Jacquey, S. Bonhommeau, P. Zahariev, A. Monmayrant, B. Chatel, and B. Girard, J. Phys. IV **119**, 13 (2004).
[6] S. L. McCall and E. L. Hahn, Phys. Rev. **183**, 457 (1969).
[7] M. D. Crisp, Phys. Rev. A **1**, 1604 (1970).
[8] D. J. Kaup and L. R. Scacca, J. Opt. Soc. Am. **70**, 224 (1980).
[9] U. Kallmann, S. Brattke, and W. Hartmann, Phys. Rev. A **59**, 814 (1999).
[10] H.-J. Hartmann and L. Laubereau, J. Chem. Phys. **80**, 4663 (1984).
[11] J. E. Rothenberg, D. Grischkowsky, and A. C. Balant, Phys. Rev. Lett. **53**, 552 (1984).
[12] J. Arlt, C. Weiss, G. Torosyan, and R. Beigang, Phys. Rev. Lett. **79**, 4774 (1997).
[13] R. Netz, T. Feurer, and J. A. Fülöp, Phys. Rev. A **64**, 043808 (2001).
[14] M. A. Bouchene, Phys. Rev. A **66**, 065801 (2002).
[15] J. Xiao, Z. Wang, and Z. Xu, Phys. Rev. A **65**, 031402(R) (2002).
[16] N. Dudovich, D. Oron, and Y. Silberberg, Phys. Rev. Lett. **88**, 123004 (2002).
[17] D. Felinto, C. A. C. Bosco, L. H. Acioli, and S. S. Vianna, Opt. Commun. **215**, 69 (2003).
[18] D. Felinto, L. H. Acioli, and S. S. Vianna, Phys. Rev. A **70**, 043403 (2004).
[19] A. Marian, M. C. Stowe, J. R. Lawall, D. Felinto, and J. Ye, Science **306**, 2063 (2004).
[20] M. C. Stowe, M. J. Thorpe, A. Pe'er, J. Ye, J. E. Stalnaker, V. Gerginov, and S. A. Diddams, Adv. At. Mol., Opt. Phys. **55**, 1 (2008).
[21] D. Aumiler, T. Ban, H. Skenderović, and G. Pichler, Phys. Rev. Lett. **95**, 233001 (2005).
[22] T. Ban, D. Aumiler, H. Skenderović, and G. Pichler, Phys. Rev. A **73**, 043407 (2006).
[23] D. Aumiler, T. Ban, and G. Pichler, Phys. Rev. A **79**, 063403 (2009).
[24] T. Ban, D. Aumiler, H. Skenderović, S. Vdović, N. Vujičić, and G. Pichler, Phys. Rev. A **76**, 043410 (2007).
[25] D. Aumiler, T. Ban, N. Vujičić, S. Vdović, H. Skenderović, and G. Pichler, Appl. Phys. B: Lasers Opt. (to be published).
[26] L. Allen and J. H. Eberly, *Optical Resonance and Two-Level Atoms* (Wiley, New York, 1975).
[27] J.-C. Diels and W. Rudolph, *Ultrashort Laser Pulse Phenomena* (Elsevier, New York, 2006).
[28] P. H. Heckmann and E. Trabert, *Introduction to the Spectroscopy of Atoms* (North-Holland, Amsterdam, 1989).
[29] M. Maric, J. J. McFerran, and A. N. Luiten, Phys. Rev. A **77**, 032502 (2008).
[30] O. Axner, J. Gustafsson, N. Omenetto, and J. D. Winefordner, Spectrochim. Acta, Part B **59**, 1 (2004).
[31] D. A. Steck, rubidium 87 D line data, http://steck.us/alkalidata
[32] W. Demtröder, *Laser Spectroscopy* (Springer-Verlag, Berlin, 2003).
[33] A. N. Nesmeyanov, *Vapor Pressures of Chemical Elements* (Elsevier, New York, 1963).
[34] P. Zhou, H. Schulz, and P. Kohns, Opt. Commun. **123**, 501 (1996).
[35] R. W. Boyd, *Nonlinear Optics* (Academic Press, San Diego, 2003).